Contrasting contribution of embryo- and postnatally-derived brain-resident macrophages in sustaining sleep-wake circuitry

Ali Seifinejad[1#*], Mojtaba Bandarabadi[2], Meriem Haddar[2],
Saskia Wundt[1], Mehdi Tafti[2], Anne Vassalli[2], Abbas Khani[3], Gianni Monaco[1*]

[1] Institute of Neuropathology, Faculty of Medicine, University of Freiburg, Freiburg, Germany
[2] Department of Biomedical Sciences, University of Lausanne, Lausanne, Switzerland
[3]Institute of Neuroinformatics, Federal Institute of Technology (ETH) Zurich, Switzerland

#Present address: Department of Biomedical Sciences, University of Lausanne, Lausanne, Switzerland

[*]Correspondence to:
Dr. Ali Seifinejad: ali.seifinejad@mail.ch or
Dr. Gianni Monaco: mongianni1@gmail.com

Summary

Sleep is a complex behavior regulated by various brain cell types. However, the roles of brain-resident macrophages, including microglia and CNS-associated macrophages (CAMs), particularly those derived postnatally, in sleep regulation remain poorly understood. Here, we investigated the effects of natural (embryo-derived) and repopulated (postnatally derived) brain-resident macrophages on the regulation of vigilance states. We found that depletion in embryonically-derived brain macrophages caused increased sleep in the active period, but reduced its quality, reflected in reduced power of brain sleep oscillations. This was observed both for the Non-REM and REM sleep stages. Subsequent repopulation by postnatal brain macrophages unexpectedly failed to reestablish normal sleep-wake patterns and additionally induced sleep fragmentation. Furthermore, brain macrophage depletion caused excitatory-inhibitory synaptic imbalance, which was resistant to repopulation, and led to increased inhibitory synapses. At the metabolite level, the distinct metabolite profile induced by brain macrophage depletion largely returned to normal after repopulation. Our findings suggest a so far largely unknown interaction between brain-resident macrophages and sleep and emphasizes striking functional differences between embryonic and postnatally-derived brain macrophages, paving the way to future exploration of the role of brain macrophages of different origin in sleep disorders and synaptic connectivity.

Keywords: Microglia, CAMs, EEG, vigilance states, sleep, synapse

48 **Introduction**

49 Sleep is a complex behavior essential for the normal functioning of animals, consistently
50 linked to various diseases when compromised[1]. Sleep regulation involves circadian and
51 homeostatic processes, determining respectively sleep timing and sleep need [2].

52 Sleep oscillatory patterns rely on the intricate connectivity of the central nervous system (CNS)
53 at synaptic and neurotransmitter levels. Various cell types, primarily neuronal populations
54 located in the hypothalamus, brainstem (BS), and basal forebrain (BF), interact to finely
55 regulate sleep. The expression of synaptic proteins increases during wakefulness and sleep
56 loss, and decreases during sleep[3], and the postsynaptic protein HOMER1A is a well-
57 established core brain molecular correlate of sleep loss [4]. Additionally, the release of key
58 neuropeptides and neurotransmitters such as HCRT (also called Orexin), serotonin (5HT),
59 noradrenaline (NA), and acetylcholine across different brain regions actively modulates sleep-
60 wake cycles[5]. This intricate interplay manifests in electroencephalographically (EEG)
61 measurable readouts distinguishing wakefulness, non-rapid eye movement sleep (NREMS),
62 and rapid eye movement sleep (REMS), characterized by distinct brain oscillatory activities
63 such as delta waves (0.5-4 Hz) for NREMS and theta waves (6-9 Hz) for REMS in rodents.
64 However, the contribution of non-neuronal cell types, such as brain-resident macrophages, to
65 brain oscillations and sleep architecture remains largely unexplored.

66 Brain-resident macrophages comprising parenchymal microglia and CAMs [6-8], play
67 significant roles in pathology and protecting the CNS from damage [9]. They participate in a
68 range of physiological functions including synaptic pruning, neurogenesis, immune
69 surveillance [10-12], and are derived from prenatal sources known as erythromyeloid precursors
70 that engraft into the developing CNS [13,14], facilitating the establishment of neuronal networks
71 especially in the first postnatal weeks [10]. If embryo-derived brain-resident macrophage cells
72 are depleted in adulthood, they repopulate from surviving endogenous cells [15]. D*e novo*
73 establishment of micoglial networks occurs by surviving cells through clonal expansion [16] and
74 these postnatal-derived microglial cells exhibit a different transcriptional signature [17].

However, whether adulthood-derived microglia exhibit functional differences relative to orginal embryo-derived populations is hotly disputed.

There is evidence that immune system activation, such as during illness, results in increased sleepiness, suggesting an interaction between the immune system and the sleep-wake cycle [18,19]. Brain-resident macrophages, being the closest immune components to sleep-regulating centers in the brain, might play a crucial role in this interaction. While some studies have demonstrated a clear influence of sleep loss on embryo-derived microglia [20-22], the opposite relationship and how the brain-resident macrophages modulate sleep/wake cycle and vigilance states remain largely unexplored. Therefore, it is essential to thoroughly investigate the extent to which brain-resident macrophages influence sleep states and brain activity during these states. EEG-recorded brain activity will therefore be an important indicator of the effects of the immune system on brain oscillations. Additionally, the influence of brain macrophages on sleep-regulating neurotransmitters, and synaptic connectivity warrants further exploration. Finally, it remains unclear whether adulthood-derived brain-resident macrophages are capable of re-establishing neural circuitries in the same manner as prenatal cells, including synaptic plasticity and neurochemical balance, which are crucial for normal sleep regulation.

Here, we undertook to address these questions through a sound experimental design and in-depth analyses. Using a comprehensive characterization of EEG signals recorded from the mice brain, we first explored whether the absence of embryo-derived brain-resident macrophages influences sleep-related brain oscillatory patterns. Next, we studied whether repopulated postnatal macrophages can normalize these patterns. Finally, we investigated how the absence and re-presence of microglia and CAMs affects brain network connectivity and neurochemistry. Our data show functional differences between embryo-derived and postnatally adulthood-derived brain-resident macrophages.

Results

Repopulated postnatally-derived brain-resident macrophages are deficient in rebuilding normal NREMS circuitry

We examined to what extent embryo-derived brain-resident macrophages contribute to sleep regulation and whether postnatal-derived macrophages mirror the same functionality. To address this, we depleted microglia from the brains of mice for two weeks using colony-stimulating factor 1 receptor (CSF1R) inhibition via PLX5622 [23], and then allowed them to repopulate for four weeks (Fig. 1A). CSF1 receptor is vital for microglia survival. Antagonizing it severely depletes microglia within three days, and upon the termination of treatment, repopulation can be readily observed within a few days[17]. We observed substantial microglia depletion (>86%) after two weeks of PLX5622 treatment, and complete repopulation four weeks after withdrawal (Fig. 1B, C).

We recorded EEG signals before depletion (control), after depletion and after repopulation (Fig. 1A). Since CSF1 inhibition also depletes CAMs [24], the effects we report here are due to the depletion of both cell types, which we refer to collectively as MG. Our experimental conditions therefore included control, MG-Dep (microglia/CAM depleted), and MG-Repop (microglia/CAM repopulation). To evaluate the distribution of vigilance states, we employed our standard sleep/wake phenotyping protocol [25], with two days of baseline (which were averaged and presented as one day in the figures) and in the third day mice underwent 6 h of SD (ZT0-ZT6) and 18 h of recovery (Fig. 1D). In baseline conditions, all experimental mice demonstrated the characteristic cycling behavior, with higher levels of wakefulness during the dark period and higher levels of NREMS during the light period and exhibited the increase in NREMS amounts in response to SD (Fig. 1E, F). However, a significant NREMS increase was observed in the baseline dark period when comparing the MG-Dep to the control condition. Interestingly, the repopulation of MG did not normalize this effect (Control: 12.75±0.72 min, MG-Dep: 16.78±0.77 min, MG-Repop: 16.54±0.70 min, mean ± SEM) (Fig. 1E, F, bottom panels). Reciprocally, there was a notable reduction in wakefulness during the dark period (Fig. 1E, F, top panels).

131 To gain insight into sleep homeostatic regulation in different mouse groups and determine
132 whether increased sleep is due to increased need for sleep, we analyzed the time course of
133 NREMS EEG delta power (1-4 Hz, a recognized quantitative readout of sleep need) across
134 our 3-day recordings. All mice groups showed a typical decline in delta power during the light
135 period and a strong rebound after SD, indicating homeostatic regulation of sleep need in all
136 groups (Fig. 1G). However, the buildup in delta power during the baseline dark period was
137 significantly lower in MG-Dep and MG-Repop mice compared to WT mice (Fig. 1G). This
138 attenuation was more pronounced in MG-Repop mice and may be partly related to the
139 increased amount of sleep during the baseline dark period (Fig. 1E, lower panel). In contrast,
140 when mice were exposed to enforced wakefulness (SD), the EEG delta power increase was
141 significantly more pronounced in MG-Dep and MG-Repop than in control conditions, and again
142 this effect was more extensive in MG-Repop than in MG-Dep (Fig. 1G). Altogether, these data
143 indicate impaired buildup of homeostatic sleep need during the waking period.
144 Spectral analysis of NREMS revealed that MG-Dep mice exhibited higher slow-delta (1-2 Hz)
145 activity compared to control mice in baseline light period (Fig. 1H, left). This frequency band
146 appears particularly affected also in MG-Repop mice, as it was significantly increased in the
147 recovery light period following SD (Fig. 1I, left). The fast-delta (3-4 Hz) frequency range was
148 in contrast blunted during both baseline and recovery light periods only in the MG-Dep
149 condition (Fig. 1H, I, left). During the baseline dark period, large delta power blunting was
150 observed in both MG-Repop (1.5-3.5 Hz) and MG-Dep (3-5.5 Hz) conditions. These deficits
151 remained nearly the same during the recovery dark period, indicating that NREMS of both
152 experimental mice appears to be shallower (Fig. 1H, I, right). Collectively, it can be concluded
153 that the presence of MG is necessary for the precise regulation of fast and slow-delta power
154 as a proxy of the sleep homeostatic process. MG repopulation not only fails to restore NREMS
155 regulation but worsens it.
156 To determine whether increased NREMS duration is due to enhanced state initiation
157 (increased number of NREMS episodes) and/or to enhanced state maintenance (increased
158 NREMS episode duration), we conducted a sleep fragmentation analysis. We found that while

159 MG-Dep mice have similar sleep bout duration patterns as the control condition, MG-Repop
160 mice showed a larger number of shorter NREMS bouts (16 seconds [Control: 6.7±0.63, MG-
161 Dep: 6.8±0.7, MG-Repop: 9.84±1.12]) and 64 seconds [Control: 12.12±1.15, MG-Dep:
162 11.02±0.81, MG-Repop: 17.63±1.2]) and fewer longer NREMS bouts (>256 seconds [Control:
163 1.96±0.28, MG-Dep: 1.74±0.33, MG-Repop: 0.62±0.17]), suggesting a strong destabilization
164 of NREMS in the MG-Repop brain (Fig. 1J).
165 During NREMS, brief bursts of brain activity in the 9-16 Hz frequency range, called spindles,
166 are generated by thalamo-cortical interactions and play roles in processes such as learning,
167 memory, and cognition [26]. To determine if MG depletion and repopulation influence spindle
168 generation, we quantified spindle rate during NREMS episodes and found a significantly
169 reduced spindle rate in MG-Dep mice compared to the control condition (Fig. 1K, L; see
170 "Methods"). In contrast to other features of NREMS, MG repopulation was found to normalize
171 the occurrence rate of spindle events, indicating that MG repopulation partially rescues the
172 circuit deficits seen after MG depletion.
173 Altogether, these data suggest that embryo-derived MG are an integral part of NREMS
174 establishment and maintenance, and repopulated postnatal MG largely fail to fulfill the normal
175 NREMS regulatory functions of embryo-derived MG.
176
177 **Depletion of brain-resident macrophages prolongs REMS and degrades its quality**
178 Different neural pathways and neurotransmitters regulate REMS compared to NREMS.
179 However, the role of MG in the regulation of REMS is not well understood. We quantified
180 REMS amount across the dark/light periods and found that MG-Dep mice display more REMS
181 compared to the control and MG-Repop conditions during the baseline dark period (Control:
182 0.67±0.1, MG-Dep: 1.17±0.21 min/h, mean ± SEM). However, in contrast to NREMS, MG
183 repopulation corrected the abnormal expression of REMS (MG-Repop: 0.61±0.13 min/h) (Fig.
184 2A, B). To investigate if the increase in REMS is due to the consolidation of this state, we
185 performed fragmentation analysis and found that the number of shorter REMS bouts (8 s) is
186 largely decreased (Control: 8.7±2.05, MG-Dep: 2.8±1.2, MG-Repop: 8.8±3.3) and longer

187 bouts (>2 min) are increased (Control: 1.5±0.8, MG-Dep: 6.1±1.1, MG-Repop: 4.71±1.4, mean
188 ± SEM) (Fig. 2C) in MG-Dep mice, suggesting stabilization of REMS in the absence of MG.
189 Theta oscillations dominate the EEG signal during REMS, where theta phase dynamically
190 modulates gamma amplitude in hippocampal and cortical networks [27]. We next investigated
191 the contribution of MG in theta oscillations and theta-gamma interactions. Spectral analysis of
192 REMS revealed a significant dampening of theta (6-8 Hz) power in MG-Dep mice during the
193 baseline dark period (Fig. 2D), which was restored after MG repopulation. We also found that
194 the theta-gamma coupling is significantly reduced in the MG-Dep condition compared to the
195 control. Although MG repopulation attempts to bring it back to the normal level, it fails
196 significantly (Fig. 2E, F).
197 Altogether, these findings suggest that the presence of MG is necessary for the normal
198 expression of REMS.
199
200 **Brain-resident macrophages contribute to the maintenance of active wakefulness**
201 The quality of prior wakefulness contributes to the expression of both NREMS and REMS.
202 Along these lines, a specific sub-state of prior wakefulness was recently proposed to drive
203 NREMS need [28], and some aspects of wakefulness may functionally substitute for REMS [29].
204 To investigate how wakefulness is expressed in our experimental conditions, we performed a
205 dynamic analysis of the full waking EEG spectrum across three recording days. This global
206 analysis revealed differential expression of the higher waking frequency bands during light-
207 dark cycles across three days, and most notably during enforced wakefulness (SD). As
208 suggested in Figure 3 (Fig. 3A), both MG-Dep and MG-Repop mice exhibit a large dampening
209 of the lower gamma (≈45-55 Hz) band during the baseline dark period, which is exacerbated
210 during the recovery dark period. Additionally, the MG-Dep mice exhibit a large blunting of the
211 higher gamma band (≈70-90 Hz) during SD, which partially normalizes after MG repopulation.
212 To better quantify the lower frequency bands, we performed PSD analysis and found that MG-
213 Dep mice exhibit a large increase in slow delta (1.35-1.75 Hz) activity compared to the control
214 mice (Fig. 3B).

215 Mice spend a portion of their waking time engaged in exploratory and motivated behaviors,
216 such as running, nest building, or drinking, often referred to in rodents as "active wakefulness".
217 These behaviors are associated with the EEG signature called "theta-dominated wakefulness"
218 (TDW 6.0-9.5 Hz), which has been suggested to be the principal driver of the sleep homeostat
219 [28]. We quantified TDW in our mice and found a large decrease in its amount in both MG-Dep
220 and MG-Repop mice during the baseline dark period (Fig. 3C, D). This reduction was more
221 pronounced in MG-Repop mice, which was also seen during SD (Fig. 3C, E). TDW is
222 associated with heightened gamma activity. We analyzed the time course of gamma activity
223 during wakefulness and found an increase in slow (32-45Hz) frequency bands in the MG-
224 Repop condition compared to the controls (Fig. 3F). The increase in these frequency bands
225 in MG-Repop mice is also apparent on time-frequency heat maps in Figure 3A.
226 Overall, these data suggest a significant imbalance in the theta/gamma-rich waking state in
227 both the MG-Dep and MG-Repop conditions, and appearance of heightened gamma activity
228 after MG repopulation.
229
230 **Disrupted balance of synaptic signaling upon MG depletion and repopulation**
231 Sleep is associated with changes in synaptic plasticity [30] and microglia play a substantial role
232 in synaptic functions, which are dependent on neuronal activity and vigilance states (VS)[31]. To
233 investigate whether MG depletion and repopulation induce changes in brain network
234 connectivity at the synaptic level, we analyzed a subset of excitatory and inhibitory synaptic
235 density proteins that are involved in sleep regulation, (e.g., the core brain molecular correlate
236 of sleep loss, HOMER1) in the brains of our experimental mice.
237 Using an ImageJ macro, we counted the number of synapses on cortical and hypothalamic
238 neurons (Fig. 4A, B) and found that the number of excitatory VGLUT1-HOMER1 synapses on
239 NEUN$^+$ cortical neurons was significantly reduced in both MG-Dep and MG-Repop conditions.
240 This reduction was more noticeable in MG-Repop mice (Fig. 4C). Interestingly, this effect was
241 regulated at the postsynaptic level (HOMER1-associated, Fig. 4D) rather than the presynaptic
242 level (VGLUT1-associated, Fig. 4E). Recently, cortical PV neurons have been proposed to be

243 responsible for homeostatic sleep regulation[32]. We found that the number of parvalbumin (PV)-
244 originated[33] Synaptotagmin-2-Gephyrin (Syt2-Geph) inhibitory synapses on the cortical
245 NEUN$^+$ neurons was significantly increased under the MG-Repop condition (Fig. 4F, G). This
246 increase could possibly be due to an increase in the activity of PV neurons, as we found that
247 the number of VGLUT1-HOMER1 excitatory synapses on PV neurons was significantly
248 increased under both MG-Dep and MG-Repop conditions (Fig. 4H, I). We additionally
249 investigated the changes in the count of VGLUT1-HOMER1 synapses on representative
250 hypothalamic neurons (HCRT) and found a significant decrease in the number of VGLUT1-
251 HOMER1 synapses on HCRT neurons in both MG-Dep and MG-Repop conditions (Fig. 4J,
252 K).
253 To further investigate changes in network connectivity in the brains of MG-Dep and MG-Repop
254 mice, we analyzed additional synaptic markers and sleep-specific neurotransmitter receptors
255 (e.g., receptors of monoaminergic systems and neuropeptides) on RNA extracted from cortical
256 samples of these mice. Our bulk analysis revealed that some general synaptic markers, such
257 as *Synaptophysin I* (*Syp*), are largely downregulated in both experimental mice, while *Slc17a7*
258 (encoding Vesicular glutamate transporter 1) and *Homer1* genes are significantly
259 downregulated in the cortex of the MG-Repop condition. Among the specific neurotransmitter
260 markers analyzed, the adrenergic receptor family (e.g. *Adrb2*, *Adra2a*, *Adrb3*, and *Adra1a*)
261 genes showed a tendency to be less expressed in both MG-Dep and MG-Repop conditions,
262 with a marked decrease in the expression of the *Adra2a* gene. Additionally, we observed a
263 reduction in expression of *Cholinergic receptor muscarinic 2* (*Chrm2*) and the serotonergic
264 receptor *5-Hydroxytryptamine receptor 1A* (*Htr1a*) genes, which mainly occur in the brain of
265 MG-Repop mice (Fig. 4L).
266 Taken together, these data suggest that brain connectivity at the synaptic level is largely
267 impaired following the depletion of brain-resident macrophages. Repopulating the brain with
268 these macrophages not only failed to normalize connectivity but, in many cases analyzed,
269 worsened it.
270

271 **Neurotransmitter release is largely restored after the repopulation of resident**
272 **macrophages**

273 Synapses, in addition to providing structural connections in the brain, play a crucial role in
274 transmitting neurotransmitters essential for the function of complex neural systems. We
275 therefore questioned whether the levels of essential neurotransmitters involved in sleep
276 regulation are affected by the depletion and repopulation of brain-resident macrophages. We
277 conducted targeted metabolomics to analyze the neurotransmitter content and metabolite
278 reservoir of the cortex, target of most neurotransmitters and region where EEG signals are
279 acquired. Assessment of neurotransmitter content was performed using chromatography with
280 tandem mass spectrometry (LC-MS/MS) in the brain of control, as well as MG-Dep and MG-
281 Repop mice. We found that pharmacological depletion of MG led to a distinct clustering of
282 metabolites, as indicated by principal component analysis (PCA) (Fig. 5A). This suggests that
283 MG plays an important role in maintaining the overall metabolic composition of the cortex. MG
284 repopulation however restored the cortical submetabolome to a pattern similar to the one
285 observed under control experimental conditions (Fig. 5A). Univariate analysis revealed a
286 reduction in norepinephrine upon MG depletion, which was restored after repopulation (Fig.
287 5B). The concentrations of acetylcholine, choline, dopamine, and serotonin remained
288 unchanged between the experimental conditions, with a slight tendency to decrease in MG-
289 Dep condition.

290 Furthermore, we observed that MG depletion led to a marked reduction of L-2-amino adipic
291 acid (L-2-AAA), which was only partially recovered after repopulation (Fig. 5B). We also
292 analyzed the precursors of neurotransmitters and found a significant decrease in the amino
293 acids L-serine and asparagine under depleted condition, which could be restored upon MG
294 repopulation (Fig. 5C). Similarly, there was a trend towards decreased glycine and L-glutamic
295 acid content (Fig. 5C).

296 Taken together, our data suggest that while network connectivity is significantly impaired in
297 MG-Dep condition and resistant to MG repopulation, the underlying substrates
298 (neurotransmitters and metabolites) are largely restored after MG repopulation.

299

300 **Discussion**

301 In this study, we investigated the extent to which embryo-derived brain-resident macrophages
302 contribute to sleep regulation and whether postnatally derived ones serve a similar role. We
303 demonstrate that MG depletion has a significant impact on the homeostatic regulation of sleep.
304 The brain circuits most vulnerable to microglia depletion and repopulation, causing the
305 changes in sleep EEG that we document, are still unknown. However, changes in slow-delta
306 activity in NREM sleep, state stabilization and reduced theta power in REMS, as well as
307 changes in waking slow-delta activity, were reported in mice with defects in hypothalamic
308 HCRT and brainstem serotonergic and noradrenergic systems[25,28,34,35]. This is suggestive of
309 functionally important local interactions between microglial populations and sleep regulating
310 circuits, as mentioned above.

311 We showed that the changes in sleep patterns after MG depletion are not fully reversed after
312 MG repopulation. Previous studies have shown that the brain global transcriptomes are little
313 influenced by repopulated microglia [17]. Furthermore, it has been suggested that after MG
314 repopulation, neuroprotection is achieved through IL-6 induction by neurons[36]. Other studies
315 reported full functionality of retinal microglia after repopulation, including continuous retinal
316 surveillance, maintenance of synaptic structure, and normal behavioral and physiological
317 responses to retinal injury [37]. However, our data reveal that MG repopulation not only fails to
318 completely restore various aspects of sleep regulation, but in some cases exacerbates altered
319 parameters, such as fragmentation of NREMS and dysregulation of sleep need. This
320 demonstrates striking funtional differences between microgial cells derived from pre-or
321 postantal sources. We speculate that not all microglia-neuronal interactions are properly
322 reestablished by adulthood-derived microglia after repopulation. Whether a longer
323 repopulation period might correct the abnormalities observed in our analysis warrants further
324 investigation. We observed a significant imbalance between excitatory and inhibitory
325 synapses after depletion of embryo-derived microglia and after repopulation with adult

326 microglia, with a notable increase in inhibitory synapses following repopulation. Studies in
327 juvenile mice prevously reported that microglia depletion in the developing brain significantly
328 increases the number of both excitatory (VGLUT1-HOMER1) and inhibitory (Syt2-Gephyrin)
329 synapses on cortical neurons, an effect that persisted after repopulation until P30. However,
330 in the adult (P60) brain, synapse density returned to normal control levels, suggesting that
331 depleting microglia during development causes long-lasting, albeit not permanent, effects[38].
332 Our data, however, show that depleting microglia in adulthood, and then repopulating them,
333 induces different results, with a reduction in excitatory synapses in both MG-Dep and MG-
334 Repop conditions, and an increase in inhibitory synapses in MG-Repop conditions. In the
335 developing brain, it has been suggested that MG-Dep impairs synaptic pruning processes and
336 alters related gene expression[10,38]. Whether the same process or any specific pathways are
337 induced by MG depletion and repopulation in the adult brain, such as aberrant reactivation of
338 developmental programs[39], remains to be found.
339 Furthermore,other studies have suggested that microglia play a role in restraining excessive
340 neuronal activation that cannot be sufficiently suppressed by inhibitory neurons alone[40]. Our
341 results suggest that embryo-derived microglia also control excessive activity of inhibitory PV
342 neurons, but the reasons why this is not corrected with adulthood-derived microglia needs
343 further investigation.
344 Deficient synaptic neurotransmission was proposed as a potential cause for abnormal sleep
345 regulation[41]. We found here an imbalanced neurotransmitter and metabolite content of the
346 brain in mice devoid of prenatal microglia. It appears that norepinephrine neurotransmission
347 is particularly sensitive to MG deficiency, as both the levels of norepinephrine metabolites and
348 the corresponding receptors are significantly affected by MG depletion. Norepinephrine is
349 implicated in both wakefulness[42] and sleep regulation[43-45], and it has been suggested that
350 microglial surveillance process relies heavily on norepinephrine signaling[46,47]. Additionally, we
351 observed a decrease in the expression of neurotransmitter precursors such as L-serine, which
352 was mirrored by changes in the concentrations of glycine, asparagine, and glutamic acid.
353 Previous studies have proposed serine as a link between metabolism and neurotransmission

354 [48], and serine serves as a precursor for synthesizing ceramide [49], which has been suggested
355 to be essential for maintaining stable wakefulness [50].
356 Our findings indicate that MG affect vigilane state regulation via multiple pathways and play
357 a more substantial role in maintaining the physical connectivity of brain networks rather than
358 neurochemical connectivity, as MG repopulation largely restores metabolites but not
359 synapses. To gain a detailed understanding of MG regulation of sleep, it will be necessary to
360 explore local specific microglial depletion, and disruption of microglia-neuron interactions
361 using inducible systems. Additionally, investigating the separate contributions of microglia and
362 CAMs in sleep regulation using Cre lines under the promoter of *Hexb* [51] and *Mrc1* [52] genes,
363 respectively, would be a starting point. The observed vigilance state phenotypic alterations
364 may also be influenced by disruptions in central factors (such as protein phosphorylation
365 orchestrated by microglial TNF-α)[53], and peripheral players (since CSF1R inhibition also
366 effects circulating and tissue macrophages)[54] warranting further investigations. Overall, our
367 results shed new light on the complex interaction between the neuroimmune system and sleep
368 regulation, and it paves the way for future investigations in this important physiopathological
369 field.
370

371 **Data availability**

372 All data are available from the corresponding author upon reasonable request.

373 **Acknowledgements**

374 We extend our gratitude to the Metabolomics Core Facility at the Department of General
375 Pediatrics, University of Freiburg, with special thanks to Dr. Luciana Hannibal and Victoria
376 Wingert for their invaluable support and expertise. AS was supported by Novartis Foundation
377 for medical-biological Research (#23B079). MB was supported by the Swiss National Science
378 Foundation (grant 190605). MT was supported by Swiss NSF (grant 201235), and the State
379 of Vaud (Faculty of Biology and Medicine, University of Lausanne). AV was supported by the

Swiss National Science Foundation (grant 31003A_182613). AK was supported by institute of neuroinformatics ETH-Zurich. GM was supported by H2020-MSCA-IF grant, n. 101025176.

Author contributions

AS conceptualized and designed the study. AS, MH, and SW performed experiments. AS, GM, and MB analyzed data. AS, GM, AK, AV, MT, and MB wrote the manuscript.

Declaration of interests

The authors declare no competing interests.

Methods

Animals. Wild type (C57BL/6J) mice were used in this study. All animals were between 12 and 14 weeks old during the time of experiments and animal experiments were approved by the Ministry for Nature, Environment and Consumers` Protection of the state of Baden-Württemberg and were performed in accordance to the respective national, federal, and institutional regulations. At all times, care was taken to minimize animal discomfort and avoid pain.

Gene expression analysis. For qPCR analysis, RNA extracted from the cortical samples of control, MG-Dep and MG-Repop mice. RNA was extracted using RNeasy micro kit (74004) and cDNA synthesis was performed using random hexamer primers and M-MLV Reverse Transcriptase Promega kit (M3682). SYBR green-based and Taqman probes were used to detect the gene expression. The assay was performed using a LightCycler480 (Roche).

Immunofluorescence and synapse counting. Mice were anesthetized with ketamine (100 mg per kg body weight) and xylazine (10 mg per kg body weight) followed by perfusion with 1× PBS. For histology, brains were kept overnight in 4% paraformaldehyde (PFA). Brains were then dehydrated in 30% sucrose for about 48 hours and then snap-frozen on dry ice. Cryosections (14µm for synapse counting and 20µm for microglia and CAM staining) from brain tissue were prepared as free floating in PBS. The following antibodies were used to stain microgliaand synapses: Rabbit-anti-IBA1 (ab178846, abcam), anti-NEUN (ab177487, ab104224, abcam), anti-VLUT1 (135304, synaptic system), anti-HOMER1 (ABN37, Millipore), anti-Gephyrin (147318, synaptic system), anti-Synaptotagmin-2 (ZDB-ATB-081002-25, ZFIN), anti-Parvalbumin (MAB1572, Merck) and anti-HCRT-A (SC-8070). The DAPI was used to stain the nucleus. Iba1 antibody was incubated overnight at 4 °C and the primary antibodies to detect synapses were incubated for 1.45hr at room temperature. The brain cuts were incubated with secondary

414 antibodies for 1-2 hours at room temperature. Fluorescence imaging was performed with TCS SP8 X
415 (Leica Microsystems). Imaging of synapses was performed using 63X objective with zoom factor 8.
416 Iba1^{+} cells were counted using Fiji. Synapse analysis and quantification were conducted using Fiji
417 macro developed previously [55] with little modifications.
418
419 **Quantitative profiling of metabolites by liquid chromatography and mass spectrometry (LC-**
420 **MS/MS).** Mice brain tissue biopsies were thawed and homogenised with ice-cold PBS supplemented
421 with 1% protease inhibitor cocktail (Sigma Nr. P8340-5ML), using a cordless pestle motor and
422 disposable pellet mixers (VWR Nr. 47747-366). Buffer volume was adjusted to reach a target of 0.1 to
423 0.3 mg wet-tissue/mL lysis buffer. Whole tissue homogenates were aliquoted for downstream
424 measurement of total protein concentration, flash-frozen and stored at -80 ºC. Sulfur-containing
425 metabolites as well as creatinine, S-adenosylmethionine and S-adenosylhomocysteine were
426 determined according to a previously published procedure [56,57]. Lactate, TCA and glycolysis
427 intermediates and other organic acids, and folates were determined as described in previous work [58].
428 Amino acids and neurotransmitters were determined using a previously described protocol [59,60]. A
429 commercially available standardized amino acid mixture was utilized to generate a calibration curve for
430 amino acids (Amino acid standards, physiological, Sigma, Nr. A9906-10ML). Calibration curves for all
431 other metabolites were prepared from individual stock solutions prepared in house. Quantitation
432 accuracy was examined by monitoring homocysteine and methylmalonic acid concentrations in an
433 external quality control, namely, the Control Special Assays in Serum, European Research Network for
434 the evaluation and improvement of screening, diagnosis, and treatment of Inherited disorders of
435 Metabolism (ERNDIM) IQCS, SAS-02.1 and SAS-02.2 from MCA Laboratories, Winterswijk,
436 Netherlands. For all other metabolites, quantitation trueness was tested by examining metabolite
437 concentrations in plasma from a previously validated sample isolated from a healthy control individual
438 with respect to standard reference ranges, using the same calibration curves and LC-MS/MS running
439 conditions. Quantification of metabolites was carried out with Analyst® 1.7.2 software, 2022 AB Sciex.
440
441 **Treatments.** In order to eliminate cells dependent on CSF1R (MG) mice were administered a CSF1R
442 inhibitor called PLX5622 (Plexxikon). The inhibitor was combined with AIN-76A standard chow at a
443 concentration of 1,200ppm (Research Diets) and the mice were given unrestricted access to it for two
444 weeks. The control group received AIN-76A standard chow without any modifications. After two weeks
445 the PLX5622 food was replaced with control food to start repopulation of MG.
446
447 **Mice surgery, data acquisition and vigilance state analysis.** Mice surgery and data acquisition were
448 performed as previously described [25]. MATLAB scripts were created to quantify various parameters
449 related to wakefulness, NREMS and REMS. These parameters include time distribution and amount of
450 episodes, as well as the fragmentation of vigilance states, all of which were defined based on previously
451 established criteria [25]. TDW analysis was conducted following the method described by Vassalli and
452 Franken [28].
453

Power spectral analysis. Using Somnologica-3TM (Medcare) software, each 4 s epoch of the EEG signal was subjected to discrete Fourier transform to determine EEG power density (spectra 0–90 Hz at a frequency resolution of 0.25 Hz). We used artifact-free, same-state–flanked 4 s epochs to calculate the mean EEG spectral profiles for each behavioral states and time intervals. To account for differences among animals in absolute EEG power, the mean values of spectral profiles were converted into percentages relative to a baseline EEG power reference value of 100%. This reference value was determined for each mouse by summing the power within the frequency range of 0.75–47.5 Hz across all states and throughout the first day of baseline recordings. To control for differences in the amount of wakefulness, NREMS and REMS, this reference was weighted so that the relative contribution of each state was identical for all mice [61]. Time-frequency heatmaps of EEG power during wakefulness were generated using methods described previously [62].

Time-course analysis. To examine the dynamic changes of EEG power within specific frequency ranges throughout the day and night, the time-course of the activity of that frequency band was computed for 4 s epochs scored as state of interest (NREMS, REMS and wake). For this purpose, the epochs for each state were divided into percentiles, ensuring that each percentile contained a roughly equal number of epochs. The number of percentiles for NREMS and REMS were: 12 for light periods, 6 for dark periods, and 8 for the 6-h light period after SD; for waking state: 6 for light periods, 12 for dark periods, 8 for the 6-h light SD, and 4 for the 6-h light after SD. The average EEG power within the specified frequency range was computed for each percentile, and subsequently normalized based on the type of analysis. This normalization was either done relative to the total power of the baseline state or with respect to the power achieved within the delta frequency band during slow-wave sleep at ZT8-12. Like power density analysis, single epochs were excluded and only power values of the epochs that themselves, as well as the two adjacent ones, were scored as artifact-free same-state were included in the analysis.

Theta-gamma cross-frequency coupling. We used the modulation index (MI) to measure the theta-gamma phase-amplitude coupling [27,63]. Using finite impulse response filters with an order equal to three cycles of the low cutoff frequency, we first bandpass-filtered EEG signals into theta (6-11 Hz) and fast-gamma (54-90 Hz) in both forward and reverse directions to eliminate phase distortion. We then estimated instantaneous phase of theta and the envelope of fast-gamma using the Hilbert transform. Theta phase was discretized into 18 equal bins (N=18, each 20°) and the average value of fast-gamma envelope within each bin was calculated. The resulting phase-amplitude histogram (P) was compared with a uniform distribution (U) using the Kullback-Leibler distance, $D_{KL}(P,U) = \sum_{j=1}^{N} P(j) * log[P(j)/U(j)]$, and normalized by $log(N)$ to obtain the modulation index, $MI = D_{KL} / log(N)$. To explore possible coupling patterns between different pairs of low and high frequency bands, we used the comodulogram analysis [63]. We considered 16 frequency bands for phase (1-18 Hz, 1-Hz increments, 2-Hz bandwidth), and 14 frequency bands for amplitude (15-90 Hz, 5-Hz increments, 10-Hz bandwidth). MI values were then calculated for all these pairs to obtain the comodulogram graph.

494 **Detection of sleep spindles.** NREMS spindles were detected automatically using an optimized
495 wavelet-based method as previously described [26]. Briefly, the power of EEG signals within 9-16Hz was
496 estimated using the complex B-spline wavelet function, and smoothed using a 200 ms Hanning window,
497 and then a threshold equal to 3 SD (SD: standard deviation) above the mean was applied to detect the
498 potential spindle events. Events shorter than 400 ms or longer than 2 s were discarded. Using band
499 pass-filtered EEG signals in the spindle range (9–16 Hz), we automatically counted the number of
500 cycles of each detected event and excluded those with <5 cycles or more than 30 cycles. To discard
501 artefacts, events with a power in the spindle band lower than 6–8.5 Hz or 16.5–20 Hz power bands
502 were not included.
503
504 **Statistical analysis.** The specific number (n) of replicates employed in each experiment is provided in
505 the corresponding figure legends. The individuals responsible for conducting SD and scoring the sleep
506 recordings were unaware of the genotype of the animals, ensuring blinding during these procedures.
507 The results are presented as mean ± SEM or mean ± SD. Statistical analyses were conducted using
508 GraphPad Prism. The significance of comparisons was determined using one- or two-way ANOVA or
509 mix effect model followed by relevant post hoc tests and are reported in the figure legends.
510
511
512
513 **Figure legends**
514
515 **Figure 1. Essential role of MG in regulation of NREMS and associated EEG oscillations.**
516 (**A**) Schematic illustration of the experimental procedure conducted on adult mice to assess
517 the brain's electrical activity using EEG. Recordings prior to PLX5622 drug administration
518 served as controls. Mice were then fed PLX5622-containing food during 2 weeks. During the
519 final 3 days of this 2-week period, a 2nd series of recordings was conducted. Following
520 PLX5622 treatment, mice were provided control food for 4 weeks. After 4 weeks under normal
521 food, a 3rd recording was performed. All 3 recordings were performed on the same mice. (**B,**
522 **C**) PLX5622 substantially depleted the microglia from the brain within 2 weeks (compare
523 control and MG-Dep). Return to normal food repopulated microglia into the brain after 4 weeks
524 (compare MG-Dep and MG-Repop). (**D**) Recording paradigm. The first 2 days of recordings
525 served as baseline, averaged as one day. The 2nd day consisted of 6 h SD followed by 18 h
526 of recovery. (**E**) Time-course of vigilance states; Wakefulness (top) and NREMS (bottom).
527 Compared to controls (black datapoints), MG-Dep (orange datapoints) and –Repop (blue
528 datapoints) mice show a large increase in NREMS duration during the dark period both at
529 baseline and during recovery (n = 9 for control and MG-Depleted conditions and n = 6 for MG-
530 Repopulated condition, 2-way ANOVA, followed by Dunnett's test, *P < 0.05; **P < 0.01; ***P
531 < 0.001, orange and blue stars, significant differences between control and MG-Dep and MG-

532 Repop mice, respectively). Data points are shown in minutes per hour (min/h) and represent
533 the average of 2 h. (**F**) From left to right: Time in wakefulness (top) and NREMS (bottom)
534 during baseline light, dark and recovery light and dark periods (Mixed-effects analysis,
535 followed by Dunnett's test, *P < 0.05; **P < 0.01; ***P < 0.001). (**G**) Time-course of EEG delta
536 power (1–4 Hz) during the 3-day recording. EEG delta power is a proxy of sleep need. Both
537 MG-Dep and MG-Repop mice show deficiency in building up sleep need during the dark period
538 (2-way ANOVA, followed by Dunnett's test, *P < 0.05; **P < 0.01; ***P < 0.001, orange and
539 blue stars, significant differences between control and MG-Dep and MG-Repop mice,
540 respectively). (**H**) EEG power spectra of experimental mice in NREMS during baseline light
541 (left) and dark (right) periods. EEG power is expressed as % of baseline power of control
542 condition. Insets show amplification of specific EEG frequencies (2-way ANOVA, followed by
543 Dunnett's test, *P < 0.05; **P < 0.01; ***P < 0.001, orange and blue stars indicate significant
544 differences between control and MG-Depleted and MG-Repopulated mice, respectively). (**I**)
545 EEG power spectra of experimental mice in NREMS during recovery light (left) and dark (right)
546 periods. (**J**) Distribution of NREMS bout durations during baseline dark period across the
547 experimental mice. Sleep bout duration is represented on the x-axis (1-way ANOVA, followed
548 by Tukey test). (**K**) (Top) Representative time-frequency heatmap of spindles. (Bottom)
549 Representative EEG/EMG signals of a detected spindle. Dashed horizontal lines indicate
550 upper and lower thresholds used to detect spindles with wavelet energy within 9-16 Hz, and
551 dashed vertical lines indicate the start and end of the detected spindle. (**L**) Spindle rate during
552 NREMS episodes in different conditions. Spindle rate significantly decreased in MG-depleted
553 mice (mixed-effects analysis, followed by Dunnett's test, *P < 0.05; **P < 0.01; ***P < 0.001)).
554
555 **Figure 2. REMS regulation largely depends on the presence of the MG.** (**A**) Time-course
556 of REMS duration in control (black), MG-Dep (orange) and MG-Repop (blue) mouse groups.
557 MG-Dep mice exhibit a large increase in REMS time during the baseline dark period (n = 9 for
558 control and MG-Dep conditions and n = 6 for MG-Repop condition, 2-way ANOVA, followed
559 by Dunnett's test, *P < 0.05; **P < 0.01; ***P < 0.001, orange and blue stars represent
560 significant differences between control and MG-Dep and MG-Repop mice, respectively). Data
561 points are shown in minutes per hour (min/h) and represent the average of 2 h. (**B**) Time in
562 REMS during baseline dark period (mixed-effects analysis, followed by Dunnett's test, *P <
563 0.05; **P < 0.01; ***P < 0.001). (**C**) Distribution of REMs bout durations during baseline dark
564 period across 3 mouse groups. Sleep bout duration is presented as x-axis (1-way ANOVA,
565 followed by Tukey test). (**D**) EEG power spectra of all experimental mice in REMS during
566 baseline dark period. Insets show amplification for specific EEG frequencies (2-way ANOVA,
567 followed by Dunnett's test, *P < 0.05; **P < 0.01; ***P < 0.001, orange and blue stars are
568 significant differences between control mice and MG-Dep and MG-Repop mice respectively).

569 (**E**) Comodulogram graphs show the modulation index for a wide range of frequency pairs,
570 obtained from 12-h recordings of one animal in different conditions. (**F**) Normalized theta-
571 gamma coupling across 3 experimental conditions. Theta-gamma coupling is significantly
572 decreased in MG-depleted and -repopulated conditions (mixed-effects analysis, followed by
573 Dunnett's test, *P < 0.05; **P < 0.01; ***P < 0.001)).
574
575 **Figure 3. MG Repopulation fails to normalize the waking state deficits induced by MG**
576 **depletion.** (**A**) Time x frequency x power heatmap representations of the waking EEG of
577 control, MG-Dep and MG-Repop mice across the 3 recorded days (48 h baseline, 6 h sleep
578 deprivation and 18 h recovery) show large changes in higher frequency bands. (**B**) EEG power
579 spectra of experimental mice in wakefulness during baseline light and dark periods (2-way
580 ANOVA, followed by Dunnett's test, *P < 0.05; **P < 0.01; ***P < 0.001, orange star are
581 significant differences between control mice and MG-Dep mice). (**C**) Time-course of TDW
582 amounts indicates decreased TDW time during the dark period in MG-Dep and MG-Rep.
583 Datapoints are shown in min/h and represent the average of 2 h (baseline days 1 and 2 are
584 averaged), (2-way ANOVA followed by Dunnett's test, orange and blue stars are significant
585 differences between control and MG-Dep and MG-Repop mice, respectively). (**D**)
586 Quantification of time in TDW (min/h) during baseline light and dark period (mixed-effects
587 analysis, followed by Dunnett's test, *P < 0.05; **P < 0.01; ***P < 0.001). (**E**) Time in TDW
588 during SD. (**F**) Waking EEG slow-gamma (32-45 Hz) power dynamics during the 3-day
589 recording (baseline days 1 and 2 are averaged) (2-way ANOVA, followed by Dunnett's test).
590
591 **Figure 4. Large synaptic imbalance after MG depletion and repopulation.** (**A**) Schematic
592 illustration of the cell types for which the number of synapses was counted. NEUN (blue) and
593 PV (orange) positive neurons in the cortex and HCRT neurons in the hypothalamus. The
594 number of co-localized excitatory VGLUT1-HOMER1 synaptic proteins on NEUN, PV and
595 HCRT positive neurons were counted. Additionally, the number of co-localized inhibitory
596 SYT2-Gephyrin synaptic proteins on NEUN neurons were counted. (**B**) Representative image
597 depicting pre, postsynaptic proteins and their colocalization in a NEUN positive neuron.
598 Synapses (arrowheads) are marked with pink color using ImageJ macro (right). Scale bar:
599 10μm. (**C**) Number of VGLUT1-HOMER1 synapses/μm^2 of $NEUN^+$ soma. N=342 cells from
600 12 mice for control, 324 cells from 11 mice for MG-Dep, and 357 cells from 12 mice for MG-
601 Repop conditions. The data show a reduced number of these synapses in both MG-Dep and
602 MG-Repop conditions (**D**) Number of HOMER1 puncta/μm^2 of $NEUN^+$ soma. (**E**) Number of
603 VGLUT1 puncta/μm^2 of NEUN+ soma. (**F**) Number of SYT2-Gephyrin synapses/μm^2 of
604 $NEUN^+$ soma. N=299 cells from 12 mice for control, 270 cells from 11 mice for MG-Dep, and
605 306 cells from 12 mice for MG-Repop conditions. (**G**) Representative images depicting SYT2-

606 Gephyrin synapses in NEUN$^+$ cortical neuron. Large increase in these inhibitory synapses is
607 observed in the MG-Repop condition. Scale bar: 10 μm. (**H**) Distribution of PV$^+$ neurons (red)
608 in the cortex. Scale bar: 100 μm (left), 10 μm (right). (**I**) Number of vGLUT1-HOMER1
609 synapses/μm^2 of PV$^+$ soma. N=29 cells from 5 mice for control, 29 cells from 5 mice for MG-
610 Dep, and 23 cells from 4 mice for MG-Repop conditions. (**J**) Left, distribution of HCRT$^+$
611 neurons (red) in the lateral hypothalamus. Right, a HCRT$^+$ neuron stained with VGLUT1
612 (green) and HOMER1 (Cyan). Scale bar: 100 and 10 μm. (**K**) Number of VGLUT1-HOMER1
613 synapses/μm^2 of HCRT+ soma. N=70 cells from 3 mice for control, 73 cells from 3 mice for
614 MG-Dep, and 77 cells from 4 mice for MG-Repop conditions. (**L**) Gene expression of synaptic
615 proteins and neurotransmitter receptors at RNA level following MG depletion and repopulation.
616 N=3 for control and MG-Dep and n=4 for MG-Repop conditions. 1-way ANOVA, followed by
617 Tukey test, *P < 0.05; **P < 0.01; ***P < 0.001.
618
619 **Figure 5. MG repopulation largely restores the metabolite changes induced by**
620 **microglial depletion.** (**A**) PCA of targeted metabolites in cortex isolated from control (n=3),
621 MG depleted (n=3) and repopulated (n=4) mice. (**B**) LC-MS/MS assessment of the
622 neurotransmitter content in the brain of control, MG-Dep and MG-Repop mice. (**C**)
623 Downregulation of amino acids in the brain of experimental mice after MG depletion. 1-way
624 ANOVA, followed by Tukey test, *P < 0.05; **P < 0.01; ***P < 0.001.
625
626
627

References

1. Ramar, K., Malhotra, R.K., Carden, K.A., Martin, J.L., Abbasi-Feinberg, F., Aurora, R.N., Kapur, V.K., Olson, E.J., Rosen, C.L., Rowley, J.A., et al. (2021). Sleep is essential to health: an American Academy of Sleep Medicine position statement. J Clin Sleep Med. 10.5664/jcsm.9476.
2. Borbély, A.A. (1982). A two process model of sleep regulation. Hum Neurobiol *1*, 195-204.
3. Gilestro, G.F., Tononi, G., and Cirelli, C. (2009). Widespread changes in synaptic markers as a function of sleep and wakefulness in Drosophila. Science *324*, 109-112. 10.1126/science.1166673.
4. Maret, S., Dorsaz, S., Gurcel, L., Pradervand, S., Petit, B., Pfister, C., Hagenbuchle, O., O'Hara, B.F., Franken, P., and Tafti, M. (2007). Homer1a is a core brain molecular correlate of sleep loss. Proc Natl Acad Sci U S A *104*, 20090-20095. 10.1073/pnas.0710131104.
5. Saper, C.B., Chou, T.C., and Scammell, T.E. (2001). The sleep switch: hypothalamic control of sleep and wakefulness. Trends Neurosci *24*, 726-731. 10.1016/s0166-2236(00)02002-6.
6. Amann, L., Masuda, T., and Prinz, M. (2023). Mechanisms of myeloid cell entry to the healthy and diseased central nervous system. Nat Immunol *24*, 393-407. 10.1038/s41590-022-01415-8.
7. Kierdorf, K., Masuda, T., Jordão, M.J.C., and Prinz, M. (2019). Macrophages at CNS interfaces: ontogeny and function in health and disease. Nat Rev Neurosci *20*, 547-562. 10.1038/s41583-019-0201-x.
8. Prinz, M., Masuda, T., Wheeler, M.A., and Quintana, F.J. (2021). Microglia and Central Nervous System-Associated Macrophages-From Origin to Disease Modulation. Annual review of immunology *39*, 251-277. 10.1146/annurev-immunol-093019-110159.
9. Prinz, M., Jung, S., and Priller, J. (2019). Microglia Biology: One Century of Evolving Concepts. Cell *179*, 292-311. 10.1016/j.cell.2019.08.053.
10. Paolicelli, R.C., Bolasco, G., Pagani, F., Maggi, L., Scianni, M., Panzanelli, P., Giustetto, M., Ferreira, T.A., Guiducci, E., Dumas, L., et al. (2011). Synaptic pruning by microglia is necessary for normal brain development. Science (New York, N.Y.) *333*, 1456-1458. 10.1126/science.1202529.
11. Shigemoto-Mogami, Y., Hoshikawa, K., Goldman, J.E., Sekino, Y., and Sato, K. (2014). Microglia enhance neurogenesis and oligodendrogenesis in the early postnatal subventricular zone. J Neurosci *34*, 2231-2243. 10.1523/jneurosci.1619-13.2014.
12. Nimmerjahn, A., Kirchhoff, F., and Helmchen, F. (2005). Resting microglial cells are highly dynamic surveillants of brain parenchyma in vivo. Science *308*, 1314-1318. 10.1126/science.1110647.
13. Kierdorf, K., Erny, D., Goldmann, T., Sander, V., Schulz, C., Perdiguero, E.G., Wieghofer, P., Heinrich, A., Riemke, P., Hölscher, C., et al. (2013). Microglia emerge from erythromyeloid precursors via Pu.1- and Irf8-dependent pathways. Nature neuroscience *16*, 273-280. 10.1038/nn.3318.
14. Schulz, C., Gomez Perdiguero, E., Chorro, L., Szabo-Rogers, H., Cagnard, N., Kierdorf, K., Prinz, M., Wu, B., Jacobsen, S.E., Pollard, J.W., et al. (2012). A lineage of myeloid cells independent of Myb and hematopoietic stem cells. Science (New York, N.Y.) *336*, 86-90. 10.1126/science.1219179.
15. Bruttger, J., Karram, K., Wörtge, S., Regen, T., Marini, F., Hoppmann, N., Klein, M., Blank, T., Yona, S., Wolf, Y., et al. (2015). Genetic Cell Ablation Reveals Clusters of Local Self-Renewing Microglia in the Mammalian Central Nervous System. Immunity *43*, 92-106. 10.1016/j.immuni.2015.06.012.
16. Tay, T.L., Mai, D., Dautzenberg, J., Fernández-Klett, F., Lin, G., Sagar, Datta, M., Drougard, A., Stempfl, T., Ardura-Fabregat, A., et al. (2017). A new fate mapping system reveals context-dependent random or clonal expansion of microglia. Nature neuroscience *20*, 793-803. 10.1038/nn.4547.

17. Huang, Y., Xu, Z., Xiong, S., Sun, F., Qin, G., Hu, G., Wang, J., Zhao, L., Liang, Y.X., Wu, T., et al. (2018). Repopulated microglia are solely derived from the proliferation of residual microglia after acute depletion. Nat Neurosci *21*, 530-540. 10.1038/s41593-018-0090-8.
18. Ingiosi, A.M., Opp, M.R., and Krueger, J.M. (2013). Sleep and immune function: glial contributions and consequences of aging. Curr Opin Neurobiol *23*, 806-811. 10.1016/j.conb.2013.02.003.
19. Imeri, L., and Opp, M.R. (2009). How (and why) the immune system makes us sleep. Nat Rev Neurosci *10*, 199-210. 10.1038/nrn2576.
20. Tuan, L.H., and Lee, L.J. (2019). Microglia-mediated synaptic pruning is impaired in sleep-deprived adolescent mice. Neurobiol Dis *130*, 104517. 10.1016/j.nbd.2019.104517.
21. Gentry, N.W., McMahon, T., Yamazaki, M., Webb, J., Arnold, T.D., Rosi, S., Ptáček, L.J., and Fu, Y.H. (2022). Microglia are involved in the protection of memories formed during sleep deprivation. Neurobiol Sleep Circadian Rhythms *12*, 100073. 10.1016/j.nbscr.2021.100073.
22. Bellesi, M., de Vivo, L., Chini, M., Gilli, F., Tononi, G., and Cirelli, C. (2017). Sleep Loss Promotes Astrocytic Phagocytosis and Microglial Activation in Mouse Cerebral Cortex. J Neurosci *37*, 5263-5273. 10.1523/jneurosci.3981-16.2017.
23. Dagher, N.N., Najafi, A.R., Kayala, K.M., Elmore, M.R., White, T.E., Medeiros, R., West, B.L., and Green, K.N. (2015). Colony-stimulating factor 1 receptor inhibition prevents microglial plaque association and improves cognition in 3xTg-AD mice. J Neuroinflammation *12*, 139. 10.1186/s12974-015-0366-9.
24. Van Hove, H., Martens, L., Scheyltjens, I., De Vlaminck, K., Pombo Antunes, A.R., De Prijck, S., Vandamme, N., De Schepper, S., Van Isterdael, G., Scott, C.L., et al. (2019). A single-cell atlas of mouse brain macrophages reveals unique transcriptional identities shaped by ontogeny and tissue environment. Nat Neurosci *22*, 1021-1035. 10.1038/s41593-019-0393-4.
25. Seifinejad, A., Li, S., Possovre, M.L., Vassalli, A., and Tafti, M. (2020). Hypocretinergic interactions with the serotonergic system regulate REM sleep and cataplexy. Nat Commun *11*, 6034. 10.1038/s41467-020-19862-y.
26. Bandarabadi, M., Herrera, C.G., Gent, T.C., Bassetti, C., Schindler, K., and Adamantidis, A.R. (2020). A role for spindles in the onset of rapid eye movement sleep. Nat Commun *11*, 5247. 10.1038/s41467-020-19076-2.
27. Bandarabadi, M., Boyce, R., Gutierrez Herrera, C., Bassetti, C.L., Williams, S., Schindler, K., and Adamantidis, A. (2019). Dynamic modulation of theta-gamma coupling during rapid eye movement sleep. Sleep *42*, 1-11. 10.1093/sleep/zsz182.
28. Vassalli, A., and Franken, P. (2017). Hypocretin (orexin) is critical in sustaining theta/gamma-rich waking behaviors that drive sleep need. Proc Natl Acad Sci U S A *114*, E5464-e5473. 10.1073/pnas.1700983114.
29. Endo, T., Roth, C., Landolt, H.P., Werth, E., Aeschbach, D., Achermann, P., and Borbély, A.A. (1998). Selective REM sleep deprivation in humans: effects on sleep and sleep EEG. Am J Physiol *274*, R1186-1194. 10.1152/ajpregu.1998.274.4.R1186.
30. Tononi, G., and Cirelli, C. (2003). Sleep and synaptic homeostasis: a hypothesis. Brain Res Bull *62*, 143-150. 10.1016/j.brainresbull.2003.09.004.
31. Hristovska, I., Robert, M., Combet, K., Honnorat, J., Comte, J.C., and Pascual, O. (2022). Sleep decreases neuronal activity control of microglial dynamics in mice. Nat Commun *13*, 6273. 10.1038/s41467-022-34035-9.
32. Kon, K., Ode, K.L., Mano, T., Fujishima, H., Tone, D., Shimizu, C., Shiono, S., Yada, S., Garçon, J.Y., Kaneko, M., et al. (2023). Cortical parvalbumin neurons are responsible for homeostatic sleep rebound through CaMKII activation. bioRxiv, 2023.2004.2029.537929. 10.1101/2023.04.29.537929.
33. Bouhours, B., Gjoni, E., Kochubey, O., and Schneggenburger, R. (2017). Synaptotagmin2 (Syt2) Drives Fast Release Redundantly with Syt1 at the Output Synapses of Parvalbumin-Expressing Inhibitory Neurons. J Neurosci *37*, 4604-4617. 10.1523/jneurosci.3736-16.2017.

730 34. Morairty, S.R., Dittrich, L., Pasumarthi, R.K., Valladao, D., Heiss, J.E., Gerashchenko, D., and
731 Kilduff, T.S. (2013). A role for cortical nNOS/NK1 neurons in coupling homeostatic sleep drive
732 to EEG slow wave activity. Proc Natl Acad Sci U S A *110*, 20272-20277.
733 10.1073/pnas.1314762110.
734 35. Cirelli, C., Huber, R., Gopalakrishnan, A., Southard, T.L., and Tononi, G. (2005). Locus ceruleus
735 control of slow-wave homeostasis. J Neurosci *25*, 4503-4511. 10.1523/jneurosci.4845-
736 04.2005.
737 36. Willis, E.F., MacDonald, K.P.A., Nguyen, Q.H., Garrido, A.L., Gillespie, E.R., Harley, S.B.R.,
738 Bartlett, P.F., Schroder, W.A., Yates, A.G., Anthony, D.C., et al. (2020). Repopulating
739 Microglia Promote Brain Repair in an IL-6-Dependent Manner. Cell *180*, 833-846.e816.
740 10.1016/j.cell.2020.02.013.
741 37. Zhang, Y., Zhao, L., Wang, X., Ma, W., Lazere, A., Qian, H.H., Zhang, J., Abu-Asab, M., Fariss,
742 R.N., Roger, J.E., and Wong, W.T. (2018). Repopulating retinal microglia restore endogenous
743 organization and function under CX3CL1-CX3CR1 regulation. Sci Adv *4*, eaap8492.
744 10.1126/sciadv.aap8492.
745 38. Favuzzi, E., Huang, S., Saldi, G.A., Binan, L., Ibrahim, L.A., Fernández-Otero, M., Cao, Y., Zeine,
746 A., Sefah, A., Zheng, K., et al. (2021). GABA-receptive microglia selectively sculpt developing
747 inhibitory circuits. Cell *184*, 4048-4063.e4032. 10.1016/j.cell.2021.06.018.
748 39. Wilton, D.K., Dissing-Olesen, L., and Stevens, B. (2019). Neuron-Glia Signaling in Synapse
749 Elimination. Annu Rev Neurosci *42*, 107-127. 10.1146/annurev-neuro-070918-050306.
750 40. Badimon, A., Strasburger, H.J., Ayata, P., Chen, X., Nair, A., Ikegami, A., Hwang, P., Chan, A.T.,
751 Graves, S.M., Uweru, J.O., et al. (2020). Negative feedback control of neuronal activity by
752 microglia. Nature *586*, 417-423. 10.1038/s41586-020-2777-8.
753 41. Guillaumin, M.C.C., Harding, C.D., Krone, L.B., Yamagata, T., Kahn, M.C., Blanco-Duque, C.,
754 Banks, G.T., Nolan, P.M., Peirson, S.N., and Vyazovskiy, V.V. (2023). Deficient synaptic
755 neurotransmission results in a persistent sleep-like cortical activity across vigilance states in
756 mice. bioRxiv, 2023.2005.2011.540034. 10.1101/2023.05.11.540034.
757 42. Seifinejad, A., Vassalli, A., and Tafti, M. (2021). Neurobiology of cataplexy. Sleep Med Rev *60*,
758 101546. 10.1016/j.smrv.2021.101546.
759 43. Osorio-Forero, A., Cardis, R., Vantomme, G., Guillaume-Gentil, A., Katsioudi, G., Devenoges,
760 C., Fernandez, L.M.J., and Lüthi, A. (2021). Noradrenergic circuit control of non-REM sleep
761 substates. Current biology : CB *31*, 5009-5023.e5007. 10.1016/j.cub.2021.09.041.
762 44. Ma, C., Li, B., Silverman, D., Ding, X., Li, A., Xiao, C., Huang, G., Worden, K., Muroy, S., Chen,
763 W., et al. (2023). Microglia Regulate Sleep via Calcium-Dependent Modulation of
764 Norepinephrine Transmission. bioRxiv, 2023.2007.2024.550176.
765 10.1101/2023.07.24.550176.
766 45. Ma, C., Li, B., Silverman, D., Ding, X., Li, A., Xiao, C., Huang, G., Worden, K., Muroy, S., Chen,
767 W., et al. (2024). Microglia regulate sleep through calcium-dependent modulation of
768 norepinephrine transmission. Nat Neurosci *27*, 249-258. 10.1038/s41593-023-01548-5.
769 46. Stowell, R.D., Sipe, G.O., Dawes, R.P., Batchelor, H.N., Lordy, K.A., Whitelaw, B.S., Stoessel,
770 M.B., Bidlack, J.M., Brown, E., Sur, M., and Majewska, A.K. (2019). Noradrenergic signaling in
771 the wakeful state inhibits microglial surveillance and synaptic plasticity in the mouse visual
772 cortex. Nat Neurosci *22*, 1782-1792. 10.1038/s41593-019-0514-0.
773 47. Liu, Y.U., Ying, Y., Li, Y., Eyo, U.B., Chen, T., Zheng, J., Umpierre, A.D., Zhu, J., Bosco, D.B.,
774 Dong, H., and Wu, L.J. (2019). Neuronal network activity controls microglial process
775 surveillance in awake mice via norepinephrine signaling. Nat Neurosci *22*, 1771-1781.
776 10.1038/s41593-019-0511-3.
777 48. Maugard, M., Vigneron, P.A., Bolanos, J.P., and Bonvento, G. (2021). l-Serine links
778 metabolism with neurotransmission. Prog Neurobiol *197*, 101896.
779 10.1016/j.pneurobio.2020.101896.

780 49. Vávrová, K., Hrabálek, A., Dolezal, P., Holas, T., and Zbytovská, J. (2003). L-Serine and glycine
781 based ceramide analogues as transdermal permeation enhancers: polar head size and
782 hydrogen bonding. Bioorg Med Chem Lett *13*, 2351-2353. 10.1016/s0960-894x(03)00409-8.
783 50. Liu, H., Wang, X., Chen, L., Chen, L., Tsirka, S.E., Ge, S., and Xiong, Q. (2021). Microglia
784 modulate stable wakefulness via the thalamic reticular nucleus in mice. Nat Commun *12*,
785 4646. 10.1038/s41467-021-24915-x.
786 51. Masuda, T., Amann, L., Sankowski, R., Staszewski, O., Lenz, M., P, D.E., Snaidero, N., Costa
787 Jordão, M.J., Böttcher, C., Kierdorf, K., et al. (2020). Novel Hexb-based tools for studying
788 microglia in the CNS. Nat Immunol *21*, 802-815. 10.1038/s41590-020-0707-4.
789 52. Masuda, T., Amann, L., Monaco, G., Sankowski, R., Staszewski, O., Krueger, M., Del Gaudio,
790 F., He, L., Paterson, N., Nent, E., et al. (2022). Specification of CNS macrophage subsets
791 occurs postnatally in defined niches. Nature *604*, 740-748. 10.1038/s41586-022-04596-2.
792 53. Pinto, M.J., Cottin, L., Dingli, F., Laigle, V., Ribeiro, L.F., Triller, A., Henderson, F., Loew, D.,
793 Fabre, V., and Bessis, A. (2023). Microglial TNFα orchestrates protein phosphorylation in the
794 cortex during the sleep period and controls homeostatic sleep. Embo j *42*, e111485.
795 10.15252/embj.2022111485.
796 54. Lei, F., Cui, N., Zhou, C., Chodosh, J., Vavvas, D.G., and Paschalis, E.I. (2020). CSF1R inhibition
797 by a small-molecule inhibitor is not microglia specific; affecting hematopoiesis and the
798 function of macrophages. Proc Natl Acad Sci U S A *117*, 23336-23338.
799 10.1073/pnas.1922788117.
800 55. Favuzzi, E., Huang, S., Saldi, G.A., Binan, L., Ibrahim, L.A., Fernández-Otero, M., Cao, Y., Zeine,
801 A., Sefah, A., Zheng, K., et al. (2021). GABA-receptive microglia selectively sculpt developing
802 inhibitory circuits. Cell *184*, 5686. 10.1016/j.cell.2021.10.009.
803 56. Behringer, S., Wingert, V., Oria, V., Schumann, A., Grunert, S., Cieslar-Pobuda, A., Kolker, S.,
804 Lederer, A.K., Jacobsen, D.W., Staerk, J., et al. (2019). Targeted Metabolic Profiling of
805 Methionine Cycle Metabolites and Redox Thiol Pools in Mammalian Plasma, Cells and Urine.
806 Metabolites *9*. 10.3390/metabo9100235.
807 57. Bravo, A.C., Aguilera, M.N.L., Marziali, N.R., Moritz, L., Wingert, V., Klotz, K., Schumann, A.,
808 Grünert, S.C., Spiekerkoetter, U., Berger, U., et al. (2022). Analysis of S-Adenosylmethionine
809 and S-Adenosylhomocysteine: Method Optimisation and Profiling in Healthy Adults upon
810 Short-Term Dietary Intervention. Metabolites *12*, 373.
811 58. Hannibal, L., Theimer, J., Wingert, V., Klotz, K., Bierschenk, I., Nitschke, R., Spiekerkoetter, U.,
812 and Grunert, S.C. (2020). Metabolic Profiling in Human Fibroblasts Enables Subtype
813 Clustering in Glycogen Storage Disease. Front Endocrinol (Lausanne) *11*, 579981.
814 10.3389/fendo.2020.579981.
815 59. Maier, J.P., Ravi, V.M., Kueckelhaus, J., Behringer, S.P., Garrelfs, N., Will, P., Sun, N., von Ehr,
816 J., Goeldner, J.M., Pfeifer, D., et al. (2021). Inhibition of metabotropic glutamate receptor III
817 facilitates sensitization to alkylating chemotherapeutics in glioblastoma. Cell Death Dis *12*,
818 723. 10.1038/s41419-021-03937-9.
819 60. Moritz, L., Klotz, K., Grunert, S.C., Hannibal, L., and Spiekerkoetter, U. (2023). Metabolic
820 phenotyping in phenylketonuria reveals disease clustering independently of metabolic
821 control. Mol Genet Metab *138*, 107509. 10.1016/j.ymgme.2023.107509.
822 61. Franken, P., Malafosse, A., and Tafti, M. (1998). Genetic variation in EEG activity during sleep
823 in inbred mice. Am J Physiol *275*, R1127-1137. 10.1152/ajpregu.1998.275.4.R1127.
824 62. Li, S., Franken, P., and Vassalli, A. (2018). Bidirectional and context-dependent changes in
825 theta and gamma oscillatory brain activity in noradrenergic cell-specific Hypocretin/Orexin
826 receptor 1-KO mice. Sci Rep *8*, 15474. 10.1038/s41598-018-33069-8.
827 63. Tort, A.B., Kramer, M.A., Thorn, C., Gibson, D.J., Kubota, Y., Graybiel, A.M., and Kopell, N.J.
828 (2008). Dynamic cross-frequency couplings of local field potential oscillations in rat striatum
829 and hippocampus during performance of a T-maze task. Proc Natl Acad Sci U S A *105*, 20517-
830 20522. 10.1073/pnas.0810524105.

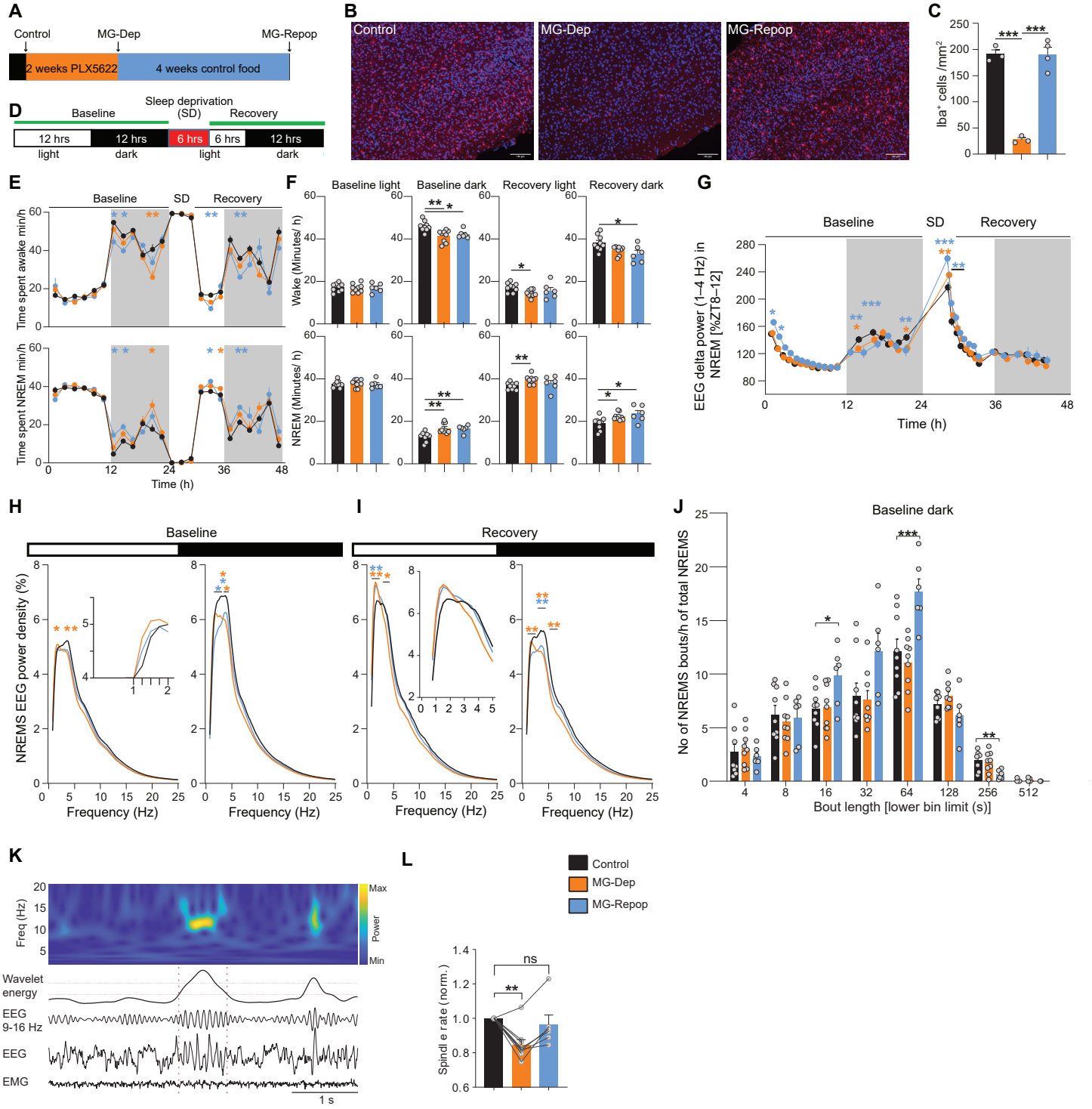
A
Control
MG-Dep
MG-Repop
2 weeks PLX5622
4 weeks control food
D
Baseline
Sleep deprivation (SD)
Recovery
12 hrs light
12 hrs dark
6 hrs light
6 hrs
12 hrs dark
B
Control
MG-Dep
MG-Repop
C
Iba+ cells /mm2
E
Baseline
SD
Recovery
Time spent awake min/h
Time spent NREM min/h
Time (h)
F
Baseline light
Baseline dark
Recovery light
Recovery dark
Wake (Minutes/ h)
NREM (Minutes/ h)
G
EEG delta power (1–4 Hz) in NREM [%ZT8–12]
Time (h)
H
Baseline
NREMS EEG power density (%)
Frequency (Hz)
I
Recovery
Frequency (Hz)
J
Baseline dark
No of NREMS bouts/h of total NREMS
Bout length [lower bin limit (s)]
K
Freq (Hz)
Max
Power
Min
Wavelet energy
EEG 9-16 Hz
EEG
EMG
1 s
L
Control
MG-Dep
MG-Repop
Spindle rate (norm.)
ns

Figure 1

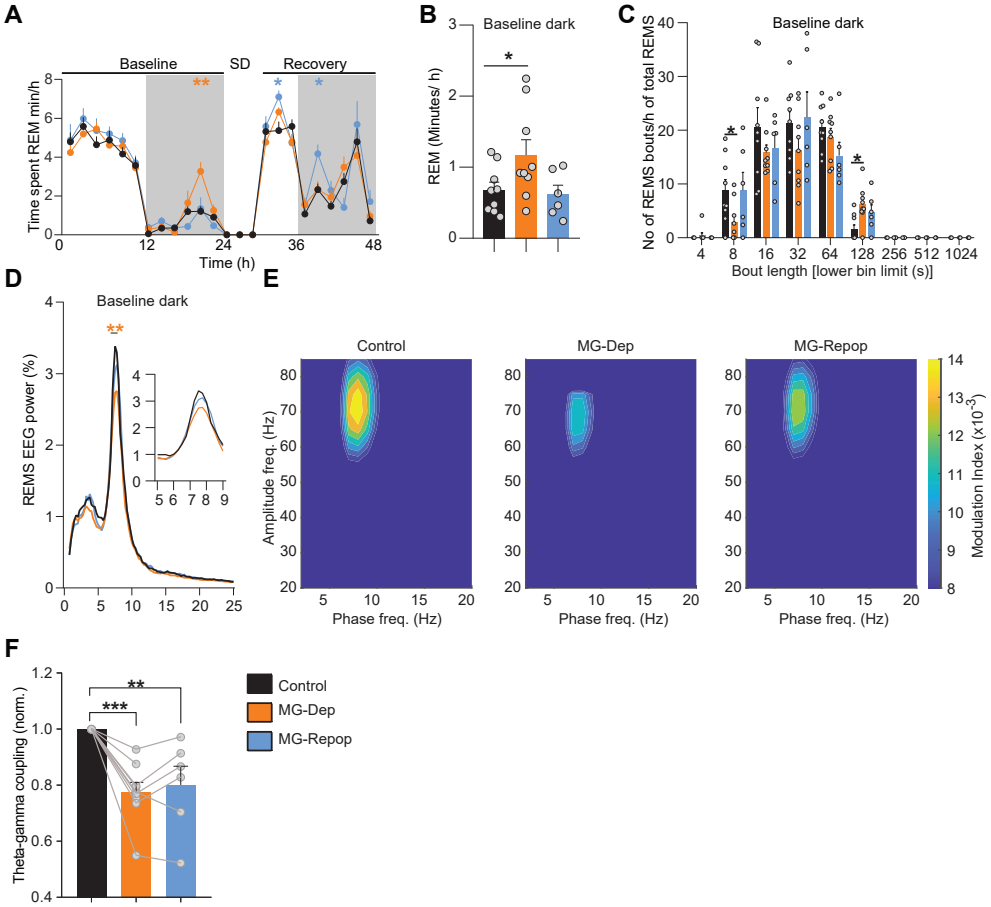
A
Baseline
SD
Recovery
Time spent REM min/h
Time (h)
B
Baseline dark
REM (Minutes/ h)
C
Baseline dark
No of REMS bouts/h of total REMS
Bout length [lower bin limit (s)]
D
Baseline dark
REMS EEG power (%)
E
Control
MG-Dep
MG-Repop
Amplitude freq. (Hz)
Phase freq. (Hz)
Modulation Index (x10-3)
F
Theta-gamma coupling (norm.)
Control
MG-Dep
MG-Repop

Figure 2

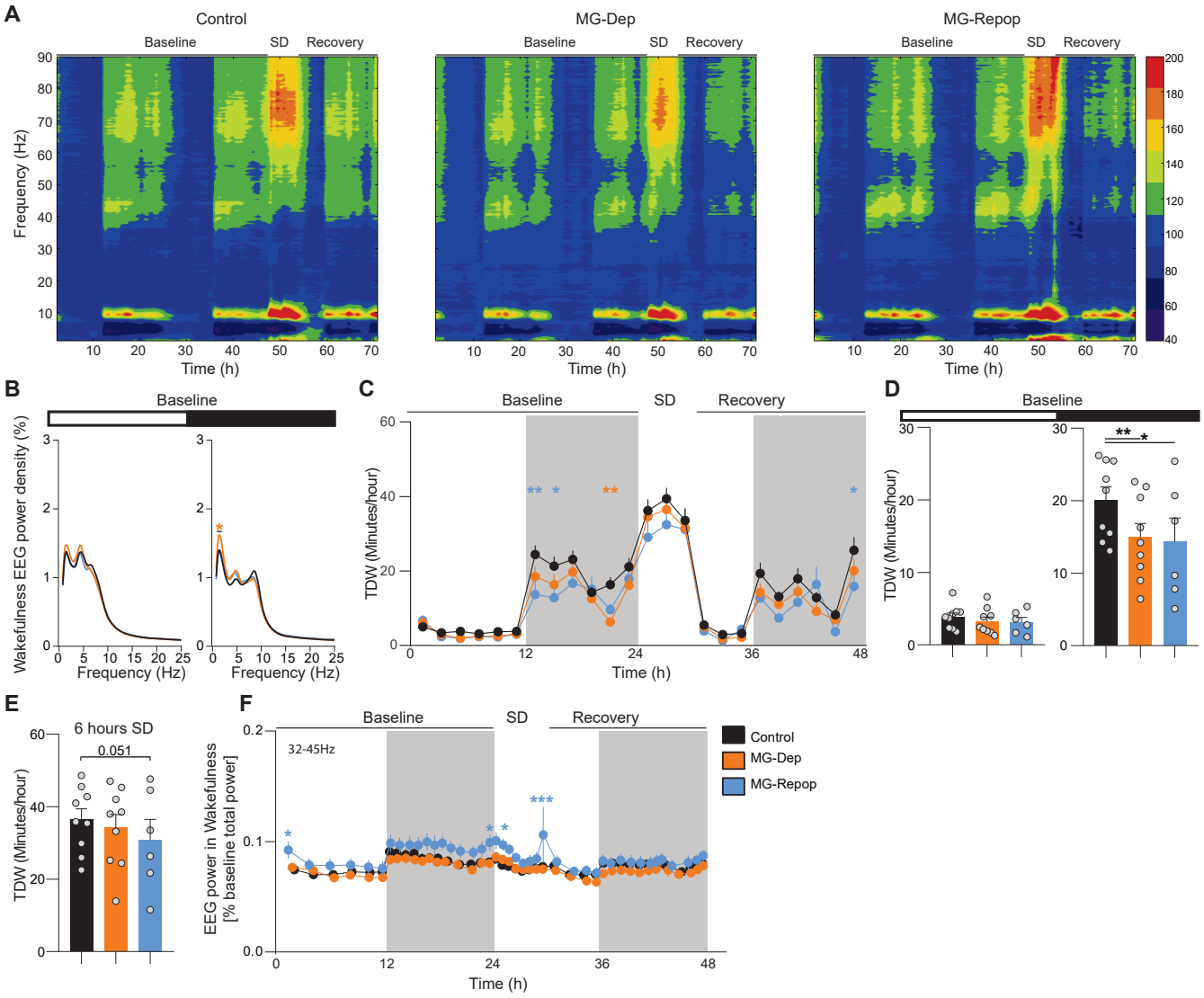
A
Control
MG-Dep
MG-Repop
Baseline
SD
Recovery
Frequency (Hz)
Time (h)
B
Wakefulness EEG power density (%)
Frequency (Hz)
C
TDW (Minutes/hour)
Time (h)
D
TDW (Minutes/hour)
E
6 hours SD
0.051
TDW (Minutes/hour)
F
32-45Hz
EEG power in Wakefulness [% baseline total power]
Time (h)
Control
MG-Dep
MG-Repop

Figure 3

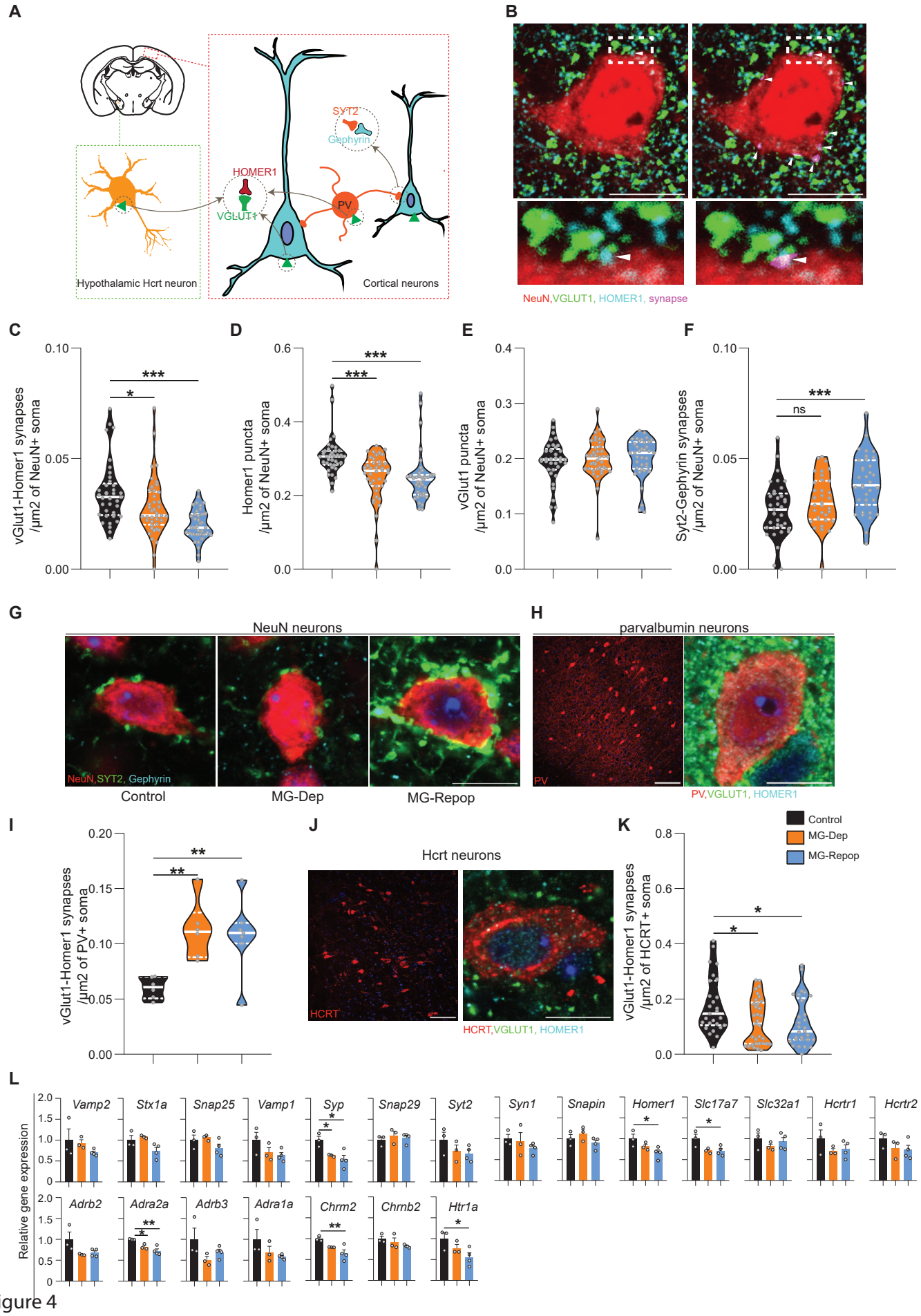
A
SYT2
Gephyrin
HOMER1
VGLUT1
PV
Hypothalamic Hcrt neuron
Cortical neurons
B
NeuN,VGLUT1, HOMER1, synapse
C
vGlut1-Homer1 synapses /µm2 of NeuN+ soma
D
Homer1 puncta /µm2 of NeuN+ soma
E
vGlut1 puncta /µm2 of NeuN+ soma
F
Syt2-Gephyrin synapses /µm2 of NeuN+ soma
ns
G
NeuN neurons
NeuN,SYT2, Gephyrin
Control
MG-Dep
MG-Repop
H
parvalbumin neurons
PV
PV,VGLUT1, HOMER1
I
vGlut1-Homer1 synapses /µm2 of PV+ soma
J
Hcrt neurons
HCRT
HCRT,VGLUT1, HOMER1
K
Control
MG-Dep
MG-Repop
vGlut1-Homer1 synapses /µm2 of HCRT+ soma
L
Relative gene expression
Vamp2
Stx1a
Snap25
Vamp1
Syp
Snap29
Syt2
Syn1
Snapin
Homer1
Slc17a7
Slc32a1
Hcrtr1
Hcrtr2
Adrb2
Adra2a
Adrb3
Adra1a
Chrm2
Chrnb2
Htr1a

Figure 4

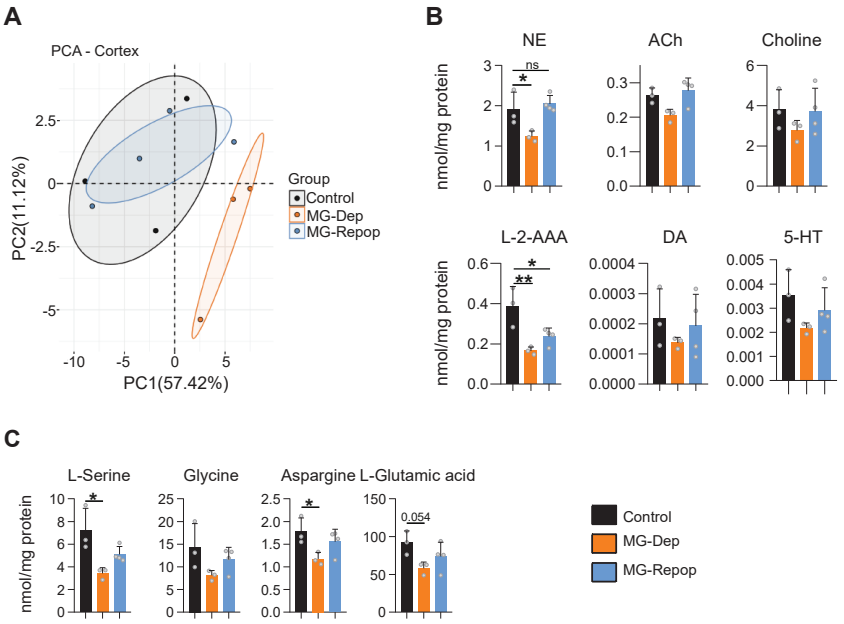
A
PCA - Cortex
PC2(11.12%)
PC1(57.42%)
Group
Control
MG-Dep
MG-Repop
B
NE
ACh
Choline
L-2-AAA
DA
5-HT
nmol/mg protein
ns
*
**
C
L-Serine
Glycine
Aspargine
L-Glutamic acid
nmol/mg protein
0.054
Control
MG-Dep
MG-Repop

Figure 5